Applied Catalysis B: Environmental 201 (2017) 479–485

Contents lists available at ScienceDirect

Applied Catalysis B: Environmental

journal homepage: www.elsevier.com/locate/apcatb

Nanotextured cupric oxide nanofibers coated with atomic layer deposited ZnO-TiO_2 as highly efficient photocathodes

Min-woo Kim[a,b,1], Hyun Yoon[a,1], Tae Yoon Ohm[a], Hong Seok Jo[a], Seongpil An[a], Sung Kyu Choi[c], Hyunwoong Park[c], Salem S. Al-Deyab[d], Byoung Koun Min[b,e], Mark T. Swihart[f], Sam S. Yoon[a,*]

[a] School of Mechanical Engineering, Korea University, Seoul 136-713, Republic of Korea
[b] Green School, Korea University, 145, Anam-ro, Seoul 02841, Republic of Korea
[c] School of Architectural, Civil, Environmental, and Energy Engineering, Kyungpook National University, Daegu 41566, Korea
[d] Petrochem. Research Chair, Dept. of Chem., King Saud Univ., Riyadh 11451, Saudi Arabia
[e] Clean Energy Research Center, Korea Institute of Science and Technology, Hwarang-ro 14-gil 5, Seongbuk-gu, Seoul 02792, Republic of Korea
[f] Dept. of Chem. & Biological Eng., University at Buffalo, The State University of New York, Buffalo, NY 14260-4200, USA

ARTICLE INFO

Article history:
Received 6 May 2016
Received in revised form 27 July 2016
Accepted 24 August 2016
Available online 24 August 2016

Keywords:
Cupric oxide nanofibers
Photocathode
Water splitting
Photocurrent density
Atomic layer deposition

ABSTRACT

We report the fabrication and performance of a CuO/ZnO/TiO_2 nanofiber photocathode that achieved a photocurrent density (PCD) of −4.1 mA/cm^2, which is among the highest PCD values reported for a copper oxide based photocathode without a co-catalyst. To prepare this photocathode, we coated electrospun nanofibers with copper by electroplating, then dried them in air to produce cuprous oxide (Cu_2O) nanofibers. Further annealing in air converted them to cupric oxide (CuO). The CuO nanofibers exhibit nanotextured surfaces, resembling the skin of the "thorny-devil" lizard of Australia, providing high accessible surface area for photocatalysis. These CuO nanofibers were uniformly coated with thin ZnO and TiO_2 layers by atomic layer deposition (ALD) to promote electron migration from CuO to TiO_2 and protect the CuO from corrosion. The nanofibrous photocathode films were characterized by X-ray diffraction, Raman spectroscopy, X-ray photoelectron spectroscopy, atomic force microscopy, scanning electron microscopy, and transmission electron microscopy, as well as by incident photon-to-electron conversion efficiency measurements.

1. Introduction

Cu_2O (cuprous oxide) and CuO (cupric oxide) have attracted considerable attention as photocathode materials for solar water splitting [1–22]. They have also shown promise in other applications, such as photovoltaics [22–31], gas sensing [32], heterogeneous catalysis [8,18,33–35], and lithium-ion batteries [36–38]. Relative to other metal oxides, such as TiO_2, ZnO, Fe_2O_3, and WO_3, Cu_2O and CuO exhibit smaller bandgaps of 2.0–2.2 eV [21] and 0.7–1.6 eV [39], respectively, allowing them to absorb a larger fraction of the solar spectrum. However, this is accompanied by disadvantages, such as low redox potential [8]. The conduction bands of Cu_2O and CuO are at −0.7 V and −0.2 V, which are relatively more negative than those of other metal oxides, making them more efficient cathodes for producing hydrogen. The theoretical maximum photocurrent densities of Cu_2O and CuO are 14.7 and 35 mA/cm^2, respectively, under AM 1.5 irradiation [17]. The Grätzel group [8] has reported a photocurrent density of 7 mA/cm^2 for their electrodeposited and atomic-layer-deposited (ALD) Cu_2O films. Multiple ZnO and TiO_2 layers together with a Pt co-catalyst were electrodeposited to produce stable Cu_2O films. Since that report, studies of copper oxides for water splitting have mainly focused on Cu_2O. Advantages of Cu_2O over CuO include the relatively large bandgap of Cu_2O (i.e., 2.0–2.2 eV), which facilitates efficient water oxidation. On the other hand, relatively few studies have been reported on CuO despite its higher chemical stability [14,21] and its higher theoretical maximum photocurrent density (PCD) associated with its narrower bandgap.

Jang et al. [19] and Masudy-Panah *et al.* [22] reported the best-performing CuO-based photocathodes to date, with PCD values of 4.4 and 2.5 mA/cm^2, respectively. Masudy-Panah et al. increased the surface area by manipulating deposition parameters during sputtering, while Jang et al. produced a complex tree-branch-

* Corresponding author.
E-mail addresses: skyoon@korea.ac.kr, skyoonsoyoung@gmail.com (S.S. Yoon).
[1] These authors have contributed equally.

http://dx.doi.org/10.1016/j.apcatb.2016.08.058
0926-3373/

shaped CuO film by electrodeposition and microwave annealing. These two studies demonstrate the importance of high surface area for increasing the PCD of CuO films.

Like those previous reports, here we produce increased surface area to achieve high PCD. However, the fabrication methodology employed here is completely different from that employed in previous studies. First, electrospun nanofibers were electroplated with copper, followed by air-drying for 24 h. This process results in the formation of sharp "thorns," resembling the skin of the thorny devil lizard [40] (Fig. 1). This thorny morphology increases the surface area and number of reaction sites. Layers of ZnO and TiO_2 were coated onto the thorny devil copper oxide to improve charge extraction and prevent CuO corrosion (Fig. 1) [41]. The flow of electrons from CuO to ZnO and TiO_2, as well as that of holes in the opposite direction, is promoted by this layered structure. At pH 14, the conduction band minima of both ZnO and TiO_2 are above 0 V, facilitating the production of hydrogen. That is, they can serve in this system as a photocathode, even though they are more commonly employed as photoanodes. Another advantage of the ZnO and TiO_2 layers is that they can protect the CuO layer from corrosion. Copper oxide is unstable as a photocathode because the redox potential for reduction of Cu_2O to Cu is 0.47 V, and the redox potential for reduction of CuO to Cu_2O is 0.60 V, both of which lie within the bandgap of CuO. This energy alignment allows photocorrosion during the reduction of water, which is undesirable. That is, photogenerated electrons, in the presence of water, can reduce copper oxide, producing Cu and OH^-, rather than reducing water to produce OH^- and H_2. ZnO and TiO_2 can prevent or mitigate corrosion because their reduction potentials (to produce Zn and OH^-, for example) do not fall within their own bandgaps and are more negative than the reduction potential of water [8]. This issue has been discussed in detail by Chan and Wang [42] who provide band-edge positions and potentials for oxidation and reduction of numerous metal oxides and other materials used as photoelectrodes.

The thickness of the TiO_2 layer was fixed at 10 nm, while that of the ZnO layer was varied from 10 to 80 nm. The optimal thickness of the ZnO layer was determined, and its overall effect on the PEC performance of the thorny devil copper nanofibers was investigated. These nanofibers were characterized by X-ray diffraction (XRD), Raman spectroscopy (Raman), X-ray photoelectron spectroscopy (XPS), atomic force microscopy (AFM), scanning electron microscopy (SEM), transmission electron microscopy (TEM), and photoelectrochemical (PEC) measurements including incident photon-to-electron conversion efficiency (IPCE) spectra.

2. Experimental

2.1. Preparation of CuO nanofibers

First, thin films of CuO with varying thickness were deposited on indium-doped tin oxide (ITO) substrates by electroplating. The electroplating solution was prepared by mixing sulfuric acid (10 g, Matsunoen Chemicals), hydrochloric acid (1 g, Sigma-Aldrich), copper sulfate (32 g, Sigma-Aldrich), formaldehyde (20 g, Sigma-Aldrich), and deionized (DI) water (200 mL). The solution was stirred for a few hours at room temperature. A bare Cu foil and the ITO substrate were used as the anode and cathode, respectively, and were entirely immersed in the electroplating solution. Table 1 summarizes the details of the electroplating process.

For deposition of the polymer nanofibers on the above CuO thin film, 6 wt% polyacrylonitrile (PAN, M_w = 150 kDa) powder was dissolved in *N*, *N*-dimethylformamide (DMF, 99.8%) by stirring for 24 h at room temperature, and the completely dissolved 6 wt% PAN solution was electrospun at a fixed flow rate of Q = 130 μL/h (Legato 100, KDS) and a DC voltage of V = 5.5–6.5 kV (EL20P2, Glassman High Voltage Inc.), as depicted in Fig. 1. The nozzle-to-substrate distance was 4.5 cm. The ambient temperature during electrospinning was 27 °C and the relative humidity level was 45%.

Table 1
Operating conditions for the electroplating process.

Items	Conditions
Applied voltage [*V*]	1
Electrode size [cm]	2.5 × 2.5 (ITO glass)4 × 3 (copper foil)
Distance between electrodes [cm]	3
Electroplating time [s]	10

Next, the nanofiber film was seeded with a few nm of platinum to provide sufficient conductivity for electroplating. The sputtered nanofiber film was electroplated a second time using the same electroplating conditions (Table 1), except that the electroplating time was changed to 15 s (cf. Fig. 1). The plated thorny devil nanofiber film was rinsed with DI water and air-dried, reinforcing the adhesion between layers and the thorny devil structure. Finally, films were heated to 500 °C at a rate of 5 °C/min in air, and held at 500 °C for 1 h.

2.2. Atomic-layer-deposition of ZnO and TiO_2 layers

To improve PEC performance, ZnO and TiO_2 layers were deposited on the CuO thorny devil films. The ZnO and TiO_2 films were fabricated by atomic layer deposition (ALD, Lucida^{TM} D series ALD, NCDtech, Korea). The ZnO layer was prepared using diethyl zinc (DEZ, EGchem) and H_2O, and the TiO_2 film was deposited from titanium(IV) isopropoxide (TTIP, EGchem) and H_2O. The temperature used in both ALD steps was 200 °C, and the overall pressure in the reactor was approximately 3×10^{-1} Torr. The ZnO deposition rate was ~0.2 nm per cycle. To study the effect of ZnO thickness, we prepared samples with 0, 10, 20, 40, and 80 nm ZnO layers. A 10 nm thick TiO_2 layer was deposited on the CuO/ZnO film at ~0.1 nm per cycle. After ALD, the CuO/ZnO/TiO_2 films were heated to 500 °C for 30 min.

2.3. Characterization

Crystal structure and crystallinity were investigated by XRD (Rigaku, Japan,D/max-2500) using Cu Kα radiation over a 2θ range of 20°–80°. The surface chemical composition of the films was investigated by XPS (Theta probe base system, Thermo Fisher Scientific Co.). The morphology of the CuO nanofibers was studied by high-resolution scanning electron microscopy (HR-SEM, XL30 SFEG, Phillips Co., Holland) at 15 kV. The thickness of films was determined by averaging values obtained from five measurements. TEM images were recorded on a JOEL-2010F system at an accelerating voltage of 200 kV. The CuO nanofibers were investigated by Raman scattering using the 532 nm (diode) line of a combined Raman and FTIR spectrometer (LabRam ARAMIS IR2, Horiba Jobin Yvon). The surface morphology of the films was characterized by atomic force microscopy (AFM, XE-100, Park System, Suwon, South Korea).

2.4. Photoelectrochemical measurements

A single cell with three electrodes was used for all PEC measurements. The CuO films were used as the working electrode, while a Ag/AgCl rod and platinum wire were used as the reference and counter electrodes, respectively. These three electrodes were placed as close as possible to one another, and their positions were fixed for acquiring consistent data and minimizing any transport limitation in the electrolyte. A 1 M KOH (pH = 14) solution was used as the electrolyte. Nitrogen gas was purged through

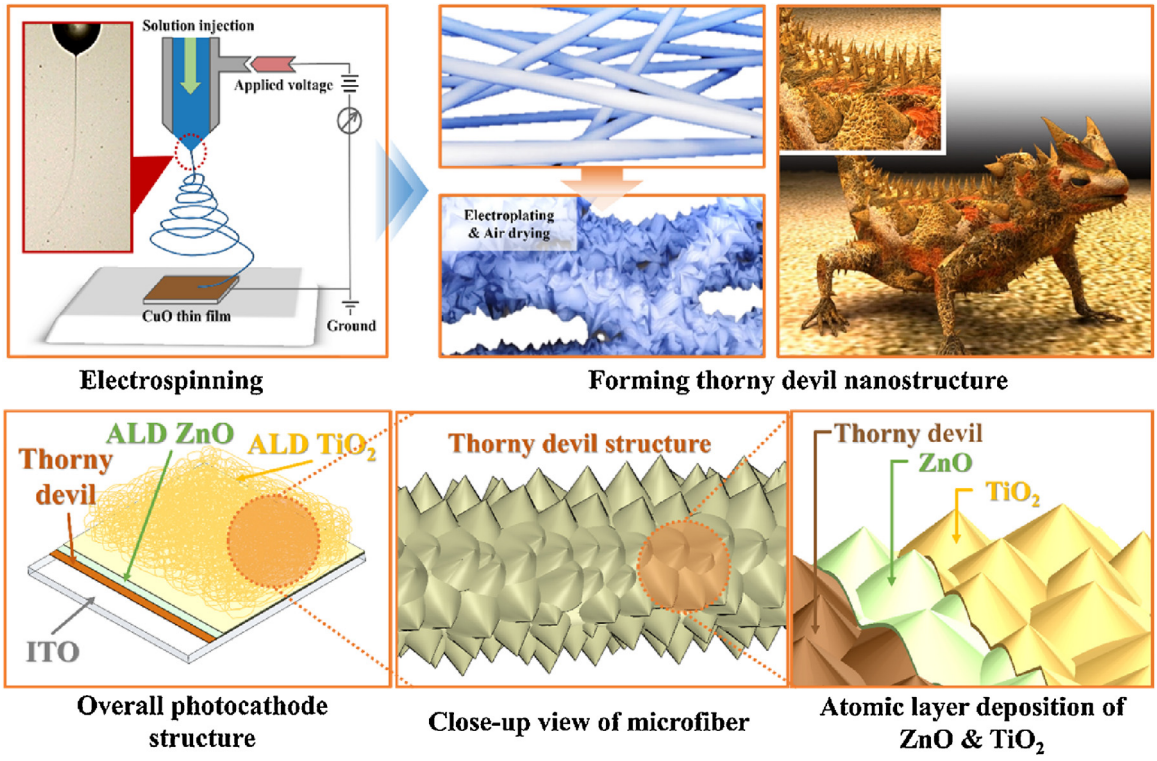

Fig. 1. Schematic of fabrication process for thorny devil CuO nanofiber thin film with ALD ZnO/TiO_2 coating.

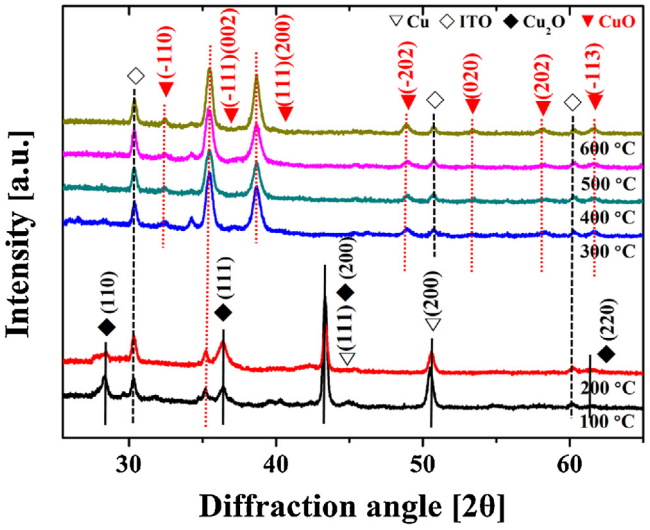

Fig. 2. XRD patterns of the copper oxide films annealed at 100–600 °C.

the electrolyte solution to remove any dissolved oxygen before measurements. Artificial sunlight from a xenon arc lamp (Newport, Oriel Instruments, USA) equipped with an AM 1.5 filter was used as the light source with an intensity of 100 mW/cm^2. All photocurrent data were recorded using a potentiostat (VersaSTAT-3, Princeton Applied Research, USA) at a scan rate of 10 mV/s with an applied voltage between 0.5 and −0.6 V relative to Ag/AgCl.

3. Results and discussion

3.1. Film characterization

Fig. 2 shows XRD patterns of the copper oxide films annealed at 100–600 °C. These films were fabricated at an electrospinning time of 60 s, an electroplating time of 15 s, and at ZnO and TiO_2 thicknesses of 40 nm and 10 nm, respectively. For the copper oxide film annealed at 100 °C, diffraction peaks were observed at 2θ values of 29.6°, 36.4°, 42.4°, and 61.4°, corresponding to the (110), (111), (200), and (220) planes of Cu_2O, respectively. Diffraction peaks were also observed at 2θ values of 30.5°, 51°, and 60.2°, attributed to the (222), (440), and (622) planes of ITO, respectively, and at 2θ values of 43.5° and 50.5°, attributed to the (111) and (200) planes of Cu, respectively, indicating the electrodeposited Cu is not fully transformed to Cu_2O even after air-drying for 24 h and post-annealing at 100 °C. A small amount of CuO was apparently formed by annealing at 100 °C; the diffraction peak at a 2θ value of 35.2° corresponds to the (−111)/(002) planes of CuO. The Cu_2O peaks diminished after annealing at 200 °C, and completely disappeared after annealing at 300 °C, beyond which only the CuO peaks were observed at 2θ values of 32.4°, 35.5°, 38.6°, 48.9°, 53.3°, 58.1°, and 61.7°, corresponding to the (−110), (−111)(002), (111)(200), (−202), (020), (202), and (−113) planes, respectively. Although the best nanofiber crystallinity was observed at 600 °C, high crystallinity may increase the crystal size beyond its optimal value, thereby decreasing the number of reaction sites for PEC reaction. The most active sites may occur at edges, vertices, and high-energy facets, which may be removed by annealing at high temperatures. Furthermore, the possibility of the diffusion of impurities from the ITO-coated soda lime glass (SLG) increases at high annealing temperature, which could increase the concentration of defect sites, promoting the recombination of charge carriers. In summary, we found that the optimal annealing temperature for maximizing photocurrent density was 500 °C; see Fig. S**2**.

Fig. 3(a)–(f) shows top-view SEM images of the electroplated and annealed nanofibers produced at electrospinning times of 0, 10, 30, 60, 120, and 180 s, respectively. The electroplating time and applied voltage were fixed at 15 s and 1 V, respectively. Electroplating for a longer time can produce overgrowth of the underlying CuO film to cover the entire fiber mat and produce a relatively

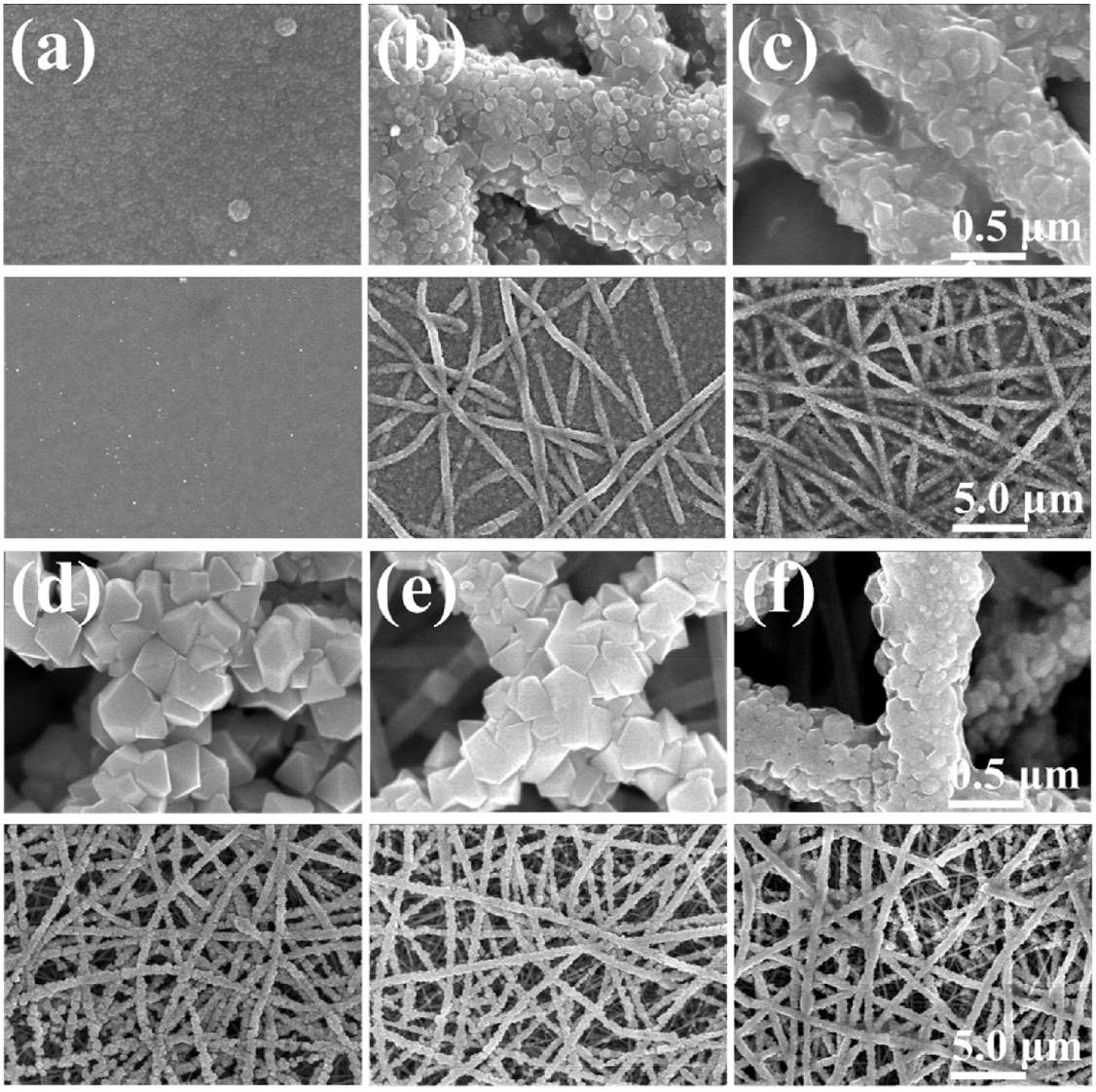

Fig. 3. Top-view SEM images of the electroplated CuO nanofibers produced at electrospinning times of 0, 10, 30, 60, 120, and 180 s for (a)–(f), respectively. These films were annealed at 500 °C.

flat surface. Thus, identifying the optimal electroplating time was essential. A thick film was formed at long electrospinning times. However, in much thicker films, only the top layer was electroplated, while bottom layers of the film remained uncoated. This can hinder the efficient transfer of electrons and holes. Thus, there is also an optimal value of the overall thickness of the fiber mat, which is determined by the electrospinning time.

As shown in Fig. 3(b)–(f), nanofibers were randomly and uniformly distributed over the substrates. Fig. 3(a), shows the planar film electroplated over the ITO-coated SLG substrate without nanofibers. All electroplated nanofibers had a similar diameter (~500 nm) as the electroplating time was maintained constant at 15 s for all cases herein. For electrospinning times of 10 and 30 s (Fig. 3(b) and (c)) this electroplating time was slightly excessive with respect to the amount of nanofibers, and some nanofibers were partially embedded in the substrate film, though not fully immersed. The nanofibers were also somewhat fused together, which could be attributed to excessive electroplating. Though the SEM images of samples produced with 60 and 120 s of electrospinning indicate similar surface structure, their PCD values differ quite significantly, as discussed further below. We believe that excessive electrospinning time produced a film whose bottom layer was not appropriately plated with copper during electroplating, which contributed to the poor electrochemical performance.

After electroplating, the nanofibers were air-dried for 24 h before annealing. After air-drying and annealing, an intrinsic nanostructure of CuO was formed, with sharp faceted crystallites. We refer to these nanostructured films after annealing as "thorny devil" nanofibers [40,43]. The nanostructuring of the fibers increases the overall surface area of the films, thereby providing a higher number of reaction sites for hydrogen evolution. At electrospinning times of t_s = 10 s and 30 s, the nanofibers were moderately textured. However, the nanofibers were highly nanotextured for t_s = 60 s and 120 s, as shown in Fig. 3(d) and (e), respectively. As shown in Fig. 3(f), an electrospinning time of t_s = 180 s was so large that the nanofibers were not sufficiently electroplated at t_p = 15 s. The grain size of CuO in this case was relatively smaller than that observed for CuO at t_s = 60 and 120 s. Thus, maximum performance is expected either at t_s = 60 or 120 s, where a sharp surface structure of CuO is formed.

Fig. 4 shows the elemental composition of the CuO nanofiber produced after annealing at 500 °C for 30 min and the subsequent coating of 40 nm thick ZnO and 10 nm thick TiO_2 layers by ALD. All the expected elements were observed in the nanofiber. The

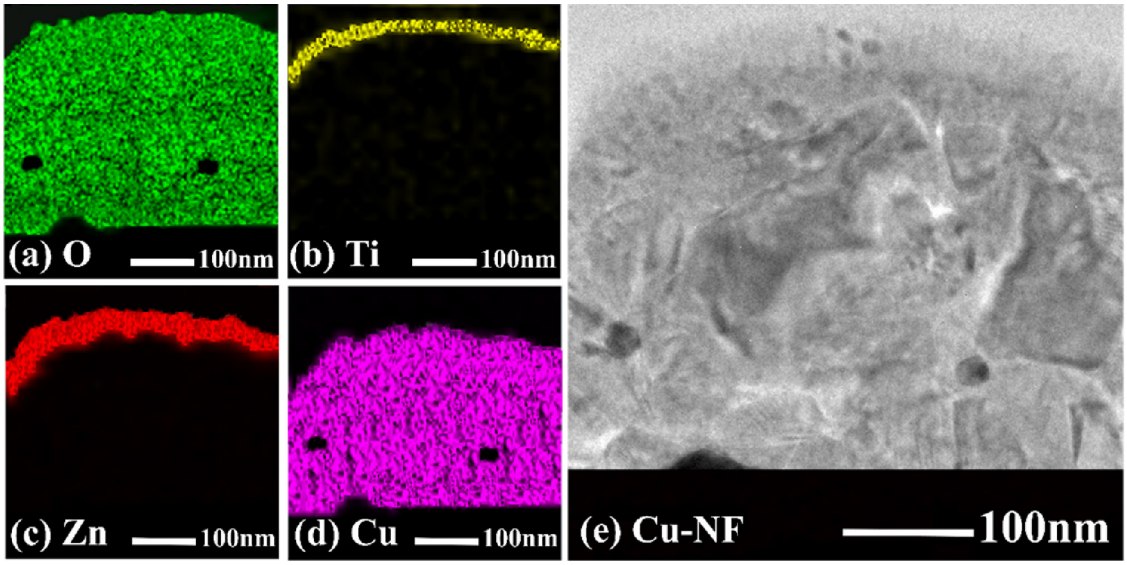

Fig. 4. Elemental composition of the CuO nanofibers for (a–d) O, Ti, Zn, and Cu, respectively. (e) Cross-sectional view of the thorny devil nanofiber observed by TEM. The nanofiber was annealed at 500 °C and then coated with 40 nm thick ZnO and 10 nm thick TiO_2 layers.

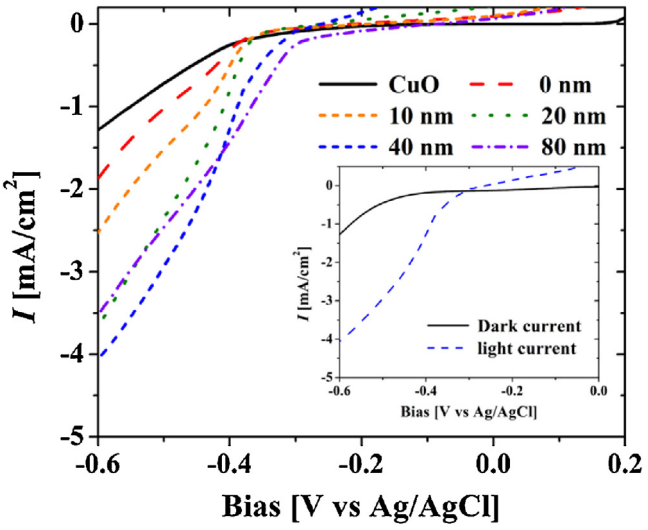

Fig. 5. Effect of the thickness of the atomic-layer-deposited ZnO layer on the photocurrent density of the CuO/ZnO/TiO_2 nanofiber. The TiO_2 layer thickness was fixed at 10 nm. Electrospinning and electroplating times were fixed at t_s = 60 s and t_p = 15 s, respectively. No co-catalyst was used.

inner region was composed of oxygen and copper (see Figs. 4(a) and (d)), on which ZnO was deposited, followed by the final outermost layer of TiO_2, which serves as a passivation layer, protecting the inner elements. The order of these elements allows for the efficient transfer of electrons from CuO to ZnO and TiO_2, as well as the transfer of holes in the opposite direction. This elemental mapping was recorded from the top part of the nanofibers; hence, PAN in the core was not investigated.

3.2. Photoelectrochemical properties

Fig. 5 shows the effect of the thickness of the ZnO layer deposited by ALD on the overall photocurrent density of the thorny-devil nanofibers when used as photocathodes for PEC water splitting in 1 M KOH (pH 14) under AM1.5 simulated solar illumination (100 mW/cm^2). Photocathode potential was measured with respect to the Ag/AgCl reference electrode, which can be converted to RHE by employing $E_{RHE} = E_{Ag/AgCl} + 0.059pH + E_{0,Ag/AgCl}$ [44]. A platinum wire was used as the counter electrode, while the CuO nanofiber film was the working photocathode. Both light and dark current–potential (I–V) curves were obtained for an optimal case of a 40 nm thick ZnO layer. The thickness of the TiO_2 layer was maintained constant at 10 nm, while that of the ZnO layer was varied from 10 to 80 nm. As shown in Fig. 5, the solid line corresponds to pure CuO without the ZnO or TiO_2 layers, attaining a PCD value of approximately −1.30 mA/cm^2 at −0.6 V. This is a higher PCD than many reports for CuO photocathodes, but the pure CuO film does not match the highest PCD values reported for CuO films by Jang et al. [19] and Masudy-Panah et al. [22]. In the absence of ZnO (i.e., 0 nm case), which corresponds to the CuO/TiO_2 structure, PCD improved to approximately −1.87 mA/cm^2, indicating the benefit of having the TiO_2 layer. With increasing thickness of the ZnO layer, PCD gradually increased, reaching a maximum value of −4.1 mA/cm^2, at which the dark current reached −1.25 mA/cm^2. Although the dark current at −0.6 V may indicate some degree of corrosion, the total photocurrent of −4.1 mA/cm^2 clearly arises mainly from PEC hydrogen generation. For the thickest ZnO layer of 80 nm, PCD decreased to approximately −3.53 mA/cm^2, indicating that a thickness of 80 nm for the ZnO layer inhibits charge carrier transport.

Under illumination in alkaline electrolyte, photoinduced electrons and holes formed in the valence band move to the conduction band. Reduction occurs when the electrons reduce H_2O to form H_2 and OH^- at the interface between solid and liquid. At the counter-electrode, OH^- is converted to H_2O and O_2, releasing electrons and completing the circuit. Here as shown in Fig. 6, the TiO_2 layer serves as a passivation layer, preventing the rapid corrosion of the CuO and ZnO layers. ZnO/TiO_2 has a type-II cascade band structure, which facilitates the flow of electrons from CuO through ZnO to the TiO_2 layer [45]. Fig. 5 shows the enhancement in the PEC performance after the insertion of the ZnO layer. The ZnO buffer layer facilitates the transport of electrons extracted from CuO toward the interface between the solid and liquid for producing H_2. The CuO/ZnO interface acts like a p–n junction, promoting the extraction of the photogenerated electrons from the p-type CuO layer to the n-type ZnO layer. As shown in Fig. 5, all of the cases with ZnO and/or TiO_2 yield PCD values greater than those obtained for pure CuO.

Fig. 7 shows the incident photon-to-current efficiency (IPCE) data at −0.6 V vs. Ag/AgCl for films annealed at 500 °C. Generally, IPCE indicates the light-harvesting capacity in the measured wave-

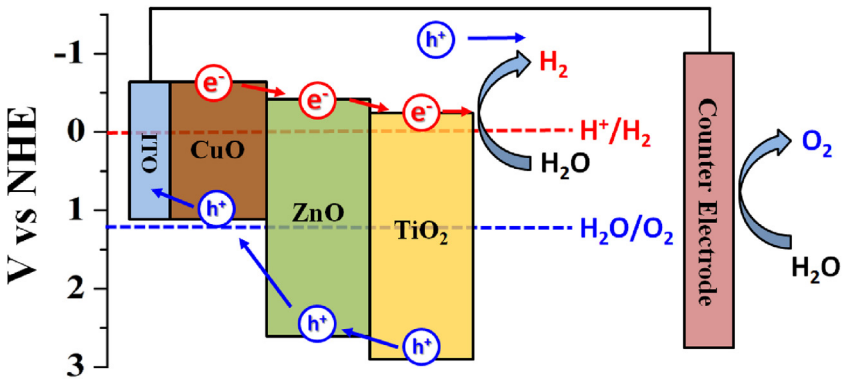

Fig. 6. Mechanism of charge transfer over the CuO/ZnO/TiO_2 photocathode.

Table 2
Comparison of the PEC performance of the present CuO thin films with literature values.

Coating method	Incident light [mW/cm^2]	Reactant solution [$CuSO_4$][a][M KOH][b][K_2SO_4][c][Na_2SO_4][d] [M $H_2BO_3^-/H_3BO_3$][e]	Applied potential [V Ag/AgCl]	pH	Photocurrent density [mA/cm^2]	Refs.
Sputtering	125	0.4[a]	−0.50	11	−0.24	[4]
Spin coating	100	1.0[b]	−0.55	14	−1.20	[35]
Spin coating	100	1.0[b]	−0.55	14	−1.20	[11]
Direct anodization	N.A.	0.5[c]	−0.36	7.29	−0.36	[15]
Spin-coating	100	0.1[d]	−0.60	5.84	−0.55	[17]
Spin coating	100	0.2[e]	−0.55	9.2	−1.50	[16]
Physical vapor deposition	100	0.5[d]	−0.50	6.4	−0.24	[21]
Hybrid microwave annealing	100	1.0[d]	−0.55	6	−4.40	[19]
Sputtering	100	0.1[d]	−0.55	5.84	−2.50	[22]
Electro-spinning/Electro-plating	**100**	**1.0**[b]	**−0.60**	14	**−4.10**	**Present work**

Note that all of the applied potential values are based on the Ag/AgCl reference potential using the following relation: $E_{RHE} = E_{Ag/AgCl} + 0.059pH + E_{0,Ag/AgCl}$ [44].

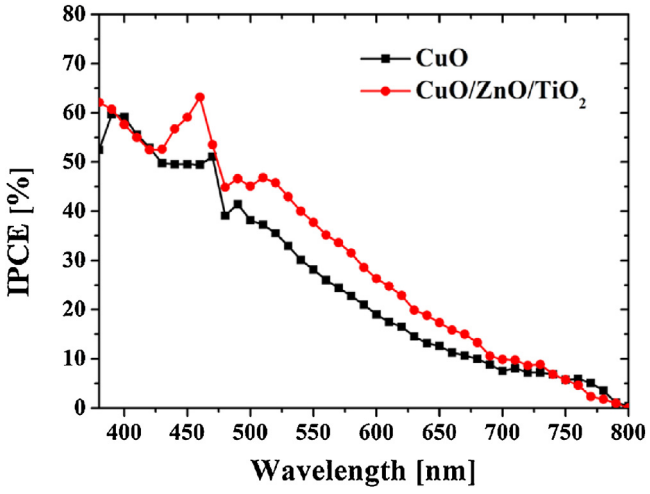

Fig. 7. IPCE spectra of CuO and CuO/ZnO/TiO_2 thin films (cathode) in 1 M KOH solution at −0.6 V vs. Ag/AgCl.

length range. Both CuO and CuO/ZnO/TiO_2 films were capable of absorbing light and separating the resulting exciton to produce photocurrent over a wide wavelength range, including both UV and visible light. Maximum IPCE values of 59.7% and 63.2% were observed at 390 and 465 nm for the CuO and CuO/ZnO/TiO_2 films, respectively. Overall, the CuO/ZnO/TiO_2 film exhibited higher IPCE than the CuO film alone over a broad wavelength range. The fact that these films cover a wide range of the solar spectrum from 380 to 800 nm is an indicator of their favorable bandgap for optimal light harvesting.

Table 2 compares the PEC performance of the current thorny devil films with prior reports of PEC using CuO. The PEC performance of the films prepared herein was better than that of most films prepared by other techniques, indicating the advantage of electrospinning and electroplating over these techniques. Jang et al. have reported the highest PCD of −4.40 mA/cm^2, attributed to the increased surface area, thereby increasing the number of photoelectrochemical reaction sites [19]. A similar route of increasing the surface area and number of reaction sites was followed here by the use of thorny-devil nanotextured surfaces. This study is the first attempt at using a nanofiber-based copper oxide material for solar water splitting. Given the large parameter space that remains to be explored for complete optimization, the proposed approach shows great promise for further improvement in future studies.

4. Conclusion

In this study, thorny-devil nanotextured cupric oxide (CuO) nanofibers were fabricated via electrospinning and electroplating and used for photoelectrochemical water splitting. Electroplated copper was oxidized to cuprous oxide (Cu_2O) by air-drying for 24 h, then annealed at an optimal annealing temperature of 500 °C in air, converting the film to CuO. These CuO nanofibers were coated with ZnO and TiO_2 by atomic layer deposition to enhance electron–hole separation and mobility, and hence photocurrent density. Indeed, the maximum photocurrent density of −4.1 mA/cm^2 was attained at an optimal thickness of 40 nm and 10 nm for ZnO and TiO_2, respectively. Given that a co-catalyst was not used, a PCD value of −4.1 mA/cm^2 was remarkably high, within 10% of the highest PCD values observed for PEC using CuO.

Acknowledgements

This research was supported by Global Frontier Program through the Global Frontier Hybrid Interface Materials (GFHIM) of NRF-2013M3A6B1078879, the Industrial Strategic Technology Development Program (10045221), and Technological Innovation R&D Program (S2314490) of the Small and Medium Business Administration (SMBA). S. S. Yoon extends his appreciation to the Vice Deanship of Scientific Research chairs at King Saud University.

Appendix A. Supplementary data

Supplementary data associated with this article can be found, in the online version, at http://dx.doi.org/10.1016/j.apcatb.2016.08.058.

References

[1] Y.S. Chaudhary, A. Agrawal, R. Shrivastav, V.R. Satsangi, S. Dass, Int. J. Hydrogen Energy 29 (2004) 131–134.
[2] J. Bandara, C.P. Udawatta, C.S. Rajapakse, Photochem. Photobiol. Sci. 4 (2005) 857–861.
[3] D. Barreca, P. Fornasiero, A. Gasparotto, V. Gombac, C. Maccato, T. Montini, E. Tondello, ChemSusChem 2 (2009) 230–233.
[4] L. Chen, S. Shet, H. Tang, H. Wang, T. Deutsch, Y. Yan, J. Turner, M. Al-Jassim, J. Mater. Chem. 20 (2010) 6962–6967.
[5] L. Wu, L,-k. Tsui, N. Swami, G. Zangari, J. Phys. Chem. C 114 (2010) 11551–11556.
[6] C.-Y. Chiang, K. Aroh, N. Franson, V.R. Satsangi, S. Dass, S. Ehrman, Int. J. Hydrogen Energy 36 (2011) 15519–15526.
[7] M. Izaki, M. Nagai, K. Maeda, F.B. Mohamad, K. Motomura, J. Sasano, T. Shinagawa, S. Watase, J. Electrochem. Soc. 158 (2011) D578–D584.
[8] A. Paracchino, V. Laporte, K. Sivula, M. Grätzel, E. Thimsen, Nat. Mater. 10 (2011) 456–461.
[9] C.-Y. Chiang, J. Epstein, A. Brown, J.N. Munday, J.N. Culver, S. Ehrman, Nano Lett. 12 (2012) 6005–6011.
[10] C.-Y. Chiang, M.-H. Chang, H.-S. Liu, C.Y. Tai, S. Ehrman, Ind. Eng. Chem. Res. 51 (2012) 5207–5215.
[11] C.-Y. Chiang, Y. Shin, K. Aroh, S. Ehrman, Int. J. Hydrogen Energy 37 (2012) 8232–8239.
[12] A. Paracchino, N. Mathews, T. Hisatomi, M. Stefik, S.D. Tilley, M. Grätzel, Energy Environ. Sci. 5 (2012) 8673–8681.
[13] M. Parmar K. Rajanna, Sensors, 2012 IEEE (2012) pp. 1–4.
[14] Z. Zhang, P. Wang, J. Mater. Chem. 22 (2012) 2456–2464.
[15] P. Wang, Y.H. Ng, R. Amal, Nanoscale 5 (2013) 2952–2958.
[16] X. Guo, P. Diao, D. Xu, S. Huang, Y. Yang, T. Jin, Q. Wu, M. Xiang, M. Zhang, Int. J. Hydrogen Energy 39 (2014) 7686–7696.
[17] Y.-F. Lim, C.S. Chua, C.J.J. Lee, D. Chi, Phys. Chem. Chem. Phys. 16 (2014) 25928–25934.
[18] C.G. Morales-Guio, S.D. Tilley, H. Vrubel, M. Grätzel, X. Hu, Nat. Commun. 5 (2014).
[19] Y.J. Jang, J.W. Jang, S.H. Choi, J.Y. Kim, J.H. Kim, D.H. Youn, W.Y. Kim, S. Han, J. Sung Lee, Nanoscale 7 (2015) 7624–7631.
[20] J. Wang, W.-D. Zhang, W.-X. Ouyang, Y.-X. Yu, Mater. Lett. 154 (2015) 44–46.
[21] P. Basnet, Y. Zhao, Catal. Sci. Technol. (2016).
[22] S. Masudy-Panah, R. Siavash Moakhar, C.S. Chua, H.R. Tan, T.I. Wong, D. Chi, G.K. Dalapati, ACS Appl. Mater. Interfaces 8 (2016) 1206–1213.
[23] S.W. Lee, Y.S. Lee, J. Heo, S.C. Siah, D. Chua, R.E. Brandt, S.B. Kim, J.P. Mailoa, T. Buonassisi, R.G. Gordon, Adv. Energy. Mater 4 (2014).
[24] Y.S. Lee, D. Chua, R.E. Brandt, S.C. Siah, J.V. Li, J.P. Mailoa, S.W. Lee, R.G. Gordon, T. Buonassisi, Adv. Mater. 26 (2014) 4704–4710.
[25] S. Masudy-Panah, G.K. Dalapati, K. Radhakrishnan, A. Kumar, H.R. Tan, J. Appl. Phys. 116 (2014) 074501.
[26] G.K. Dalapati, R.S. Kajen, S. Masudy-Panah, P. Sonar, J. Phys. D: Appl. Phys. 48 (2015) 495104.
[27] S. Masudy-Panah, K. Radhakrishnan, H.R. Tan, R. Yi, T.I. Wong, G.K. Dalapati, Sol. Energy Mater. Sol. Cells 140 (2015) 266–274.
[28] J. Katayama, K. Ito, M. Matsuoka, J. Tamaki, J. Appl. Electrochem. 34 (2004) 687–692.
[29] K. Akimoto, S. Ishizuka, M. Yanagita, Y. Nawa, G.K. Paul, T. Sakurai, Sol. Energy 80 (2006) 715–722.
[30] S. Jeong, A. Mittiga, E. Salza, A. Masci, S. Passerini, Electrochim. Acta 53 (2008) 2226–2231.
[31] J. Cui, U.J. Gibson, J. Phys. Chem. C 114 (2010) 6408–6412.
[32] P. Rai, R. Khan, S. Raj, S.M. Majhi, K.-K. Park, Y.-T. Yu, I.-H. Lee, P.K. Sekhar, Nanoscale 6 (2014) 581–588.
[33] J. Azevedo, L. Steier, P. Dias, M. Stefik, C. Sousa, J. Araujo, A. Mendes, M. Graetzel, S. Tilley, Energy Environ. Sci. 7 (2014) 4044–4052.
[34] L. Zhu, M. Hong, G.W. Ho, Nano Energy 11 (2015) 28–37.
[35] S. Gao, Y. Sun, F. Lei, J. Liu, L. Liang, T. Li, B. Pan, J. Zhou, Y. Xie, Nano Energy 8 (2014) 205–213.
[36] J. Morales, L. Sanchez, S. Bijani, L. Martınez, M. Gabas, J. Ramos-Barrado, Electrochem. Solid-State Lett. 8 (2005) A159–A162.
[37] Y. Lee, I. Leu, C. Liao, S. Chang, M. Wu, J. Yen, K. Fung, Electrochem. Solid-State Lett. 9 (2006) A207–A210.
[38] S. Bijani, M. Gabás, L. Martínez, J. Ramos-Barrado, J. Morales, L. Sánchez, Thin Solid Films 515 (2007) 5505–5511.
[39] J.W. Schultze, M. Lohrengel, Electrochim. Acta 45 (2000) 2499–2513.
[40] S. An, C. Lee, M. Liou, H.S. Jo, J.J. Park, A.L. Yarin, S.S. Yoon, ACS Appl. Mater. Interfaces 6 (2014) 13657–13666.
[41] L. Rovelli, S.D. Tilley, K. Sivula, ACS Appl. Mater. Interfaces 5 (2013) 8018–8024.
[42] S. Chen, L.-W. Wang, Chem. Mater. 24 (2012) 3659–3666.
[43] S. Sinha-Ray, Y. Zhang, A.L. Yarin, Langmuir 27 (2011) 215–226.
[44] R. Saito, Y. Miseki, K. Sayama, Chem. Commun. 48 (2012) 3833–3835.
[45] R. Marschall, Adv. Funct. Mater. 24 (2014) 2421–2440.